quaternary

MDPI

Article

Palaeogeographical Reconstruction of Ancient Diolkos Slipway by Using Beachrocks as Proxies, West Corinth Isthmus, Greece

Giannis Saitis *, Anna Karkani, Niki Evelpidou and Hampik Maroukian

Faculty of Geology and Geoenvironment, National and Kapodistrian University of Athens, Panepistimiopolis, 15784 Athens, Greece; ekarkani@geol.uoa.gr (A.K.); evelpidou@geol.uoa.gr (N.E.); maroukian@geol.uoa.gr (H.M.)
* Correspondence: saitij@geol.uoa.gr

Abstract: Beachrocks are well known as significant proxies for paleoenvironmental analysis as they indicate the coastal evolution. The combination of geomorphological and archaeological sea level indicators has a significant contribution to the coastal paleogeographic reconstruction. In this study, we studied a beachrock from the Diolkos area (West Corinth canal, Greece) and remnants of Diolkos slipway to reconstruct the coastal evolution before Diolkos construction until today. We conducted detailed mapping of Diolkos beachrock using DGPS-GNSS, as well as mineralogical analysis and OSL dating of beachrock samples. The results showed that a beachrock slab was preserved before the construction of Diolkos below it, followed by its submergence by a co-seismic event after Diolkos abandonment during 146 B.C. Consequently, a new beachrock was developed on top of the submerged Diolkos around 120 ± 14 A.D. The RSL was stable until 1596 ± 57 A.D. when the beachrock developed even closer to the present-day coastline. After 1596 A.D., it was uplifted by 12 cm until it reached today's condition.

Keywords: Corinth Gulf; geomorphology; coastal evolution; relative sea level; sea level indicator

Citation: Saitis, G.; Karkani, A.; Evelpidou, N.; Maroukian, H. Palaeogeographical Reconstruction of Ancient Diolkos Slipway by Using Beachrocks as Proxies, West Corinth Isthmus, Greece. *Quaternary* **2022**, *5*, 7. https://doi.org/10.3390/quat5010007

Academic Editor: Ioannis Liritzis

Received: 8 December 2021
Accepted: 6 January 2022
Published: 18 January 2022

1. Introduction

Research on coastal evolution is an important tool for interpreting future littoral changes in the context of climate change [1,2]. Several recent studies have used a wide variety of coastal sediments in an attempt to reconstruct late Holocene littoral changes [3–8].

Beachrocks are hard littoral deposits, which are composed of a wide variety of beach sediments that are lithified through the precipitation of carbonate cement at the shoreline [9–12]. Typically, the cement is composed of two mineralogies: high magnesium calcite (HMC) and aragonite [13]. The diagenetic environment of beachrocks may be determined by the cement mineralogy and morphology [14]; therefore, the study of these characteristics can enable defining the spatial relationship between the past coastline and the formation zone of the beachrock [10]. In fact, the cement is composed of acicular aragonite with isopachous fringes within the lower intertidal zone, or HMC cements with thin-bladed isopachous crusts, or dark or golden brown, pelletal and micritic, irregular grain coatings and void fillings [15,16].

Beachrocks are frequently used to determine late Holocene shoreline changes for the reconstruction of paleo-shorelines and as sea level indicators for the study of relative sea level changes in various coastal environments [10,12,17–22]. In the absence of other sea level indicators, especially along sandy coastlines, they can provide significant data on relative sea level changes, or even in combination with other sea level markers. Such is the case of the Aegean Sea, where beachrock occurrences are particularly common [12,18,20,22–26].

Amongst the main difficulties in the study of beachrocks, including sea level or paleogeographic indicators, is to obtain a geochronology for their development; commonly, beachrocks are dated through radiocarbon dating using shells or the cement. However, difficulties may arise as, frequently, beachrocks may have undergone more than one

diagenetic phase [9], while the cement from one single slab may provide different ages [18]. Dating marine fossils incorporated in the beachrock also facilitates errors as it has been noted that there may be an important time period between the death of the organism and its incorporation into the beachrock. In this latter case, the age obtained should be considered as the maximum [27,28]. During the past decade, luminescence dating has also been used for a variety of coastal sediments [12,29], and it has also been proven useful to obtain a geochronology for beachrock formation in the Mediterranean [12,29–31] and elsewhere [32–34].

In this context, the aim of this study is to investigate the coastal evolution of the Diolkos site at Corinth Gulf, Greece though the morphological mapping of beachrock outcrops, cement investigation, and luminescence dating.

2. Study Area

2.1. Geological and Geotectonic Setting

The study area is located at the Gulf of Corinth (Figure 1), a prominent tectonic and geomorphological structure in the central part of Greece, separating the Peloponnese to the south and central Greece to the north. The Diolkos site lies on the south coasts of the isthmus canal.

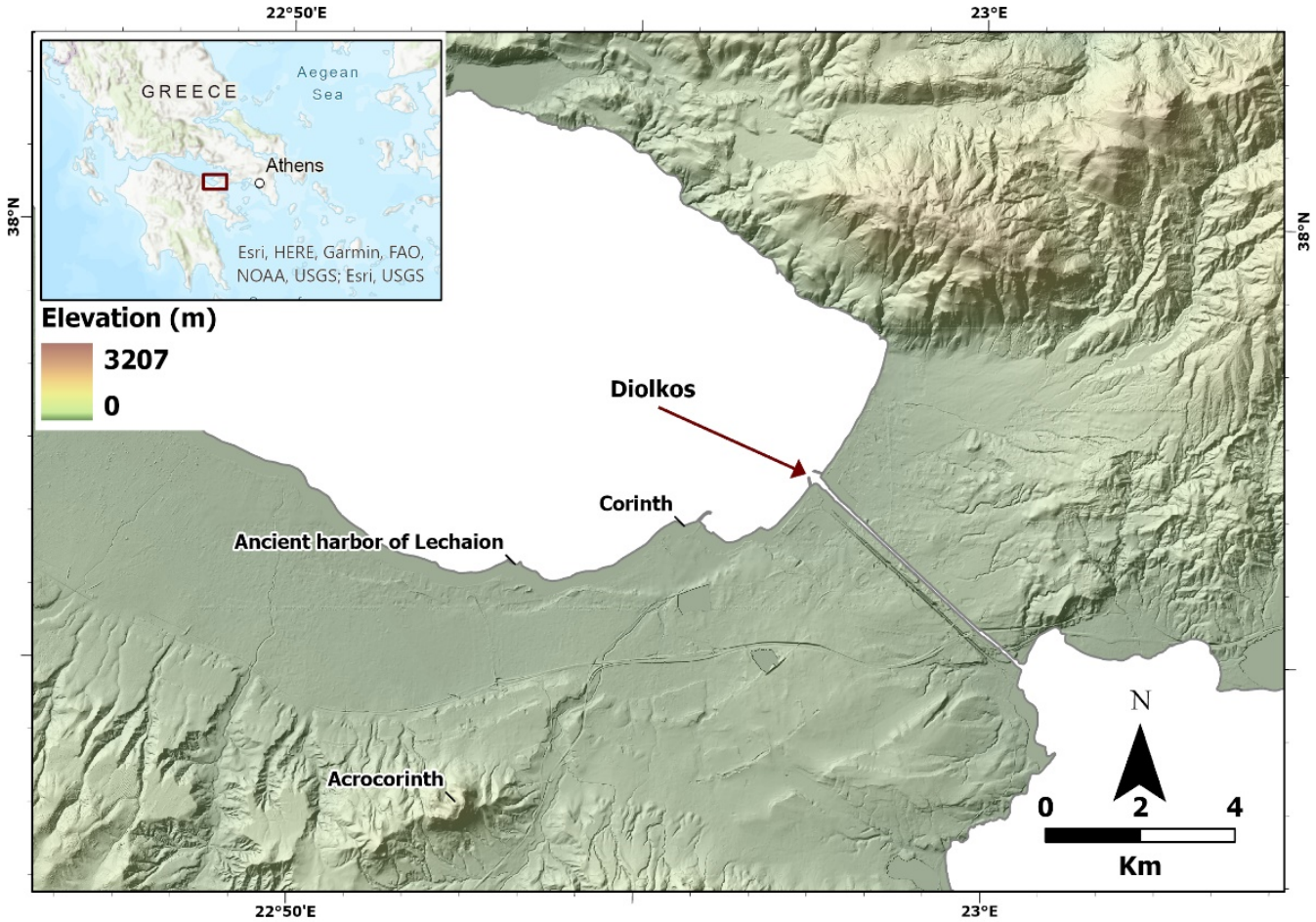

Figure 1. A morphological elevation map of the general area of Corinth. Corinth isthmus (canal) can be observed along with the modern town of Corinth, the Acrocorinth, and the ancient harbor of Lechaion.

The geological basement of Corinth is dominated by rocks of the tectonostratigraphic terrain 3 of the Hellenides [35]. The area of Corinth consists of the rocks of the sub-Pelagonian unit, a part of an old continental margin. This unit is mostly characterized by sedimentary rocks of Triassic to Jurassic grey limestones [35,36]. The topography and

geology of this area have been profoundly affected by the fault system, which follows the Central Hellenic Shear Zone extending from the Aegean part to the Ionian Sea and Peloponnese part [37]. This movement along the zone has created many grabens, one of which is the Gulf of Corinth, because of the Pliocene–Quaternary subsidence with marine sediments. The subsidence seized during the middle–lower Pleistocene when the marine sediments were uplifted and eroded.

More specifically, the Corinth canal shows a variety of sedimentary deposits, such as faulted Pliocene–Pleistocene marls, limestones, sandstones, and conglomerates [36]. These deposits can be observed at the canal internal sides [36]. These rocks were formed early in the history of the Gulf of Corinth graben when the southern part was below sea-level and were uplifted relatively recently. To the center of the canal, the oldest exposed rocks are visible. They are a series of pale marls with minor strata of brown sandstones and conglomerates and are Late Pliocene in age [36]. Both these sequences were raised above sea level through an east/west fault system. These steeply inclined normal faults are visible every few hundred meters along the canal [36,37].

From the report of the Hellenic Navy Hydrographic Service, [38] during the period of 1990–2012, the area of Diolkos showed a maximum tide of 0.72 m, a minimum of 0.01 m, and mean tide range of 0.26 m.

2.2. The Ancient Diolkos Slipway

Diolkos was a slipway used for transporting ships from the Saronic to the Corinth Gulf and in reverse. Part of the paved road was excavated by Verdelis [39,40]. The excavations at the western edge of the isthmus revealed that this road was used for transporting ships with the help of a wheeled vehicle, where the ships were moored, exempt from their cargo to the docks of Cenchreae or Lechaion. Diolkos was particularly useful for transporting warships, which had no cargo. The width of the road was 3.5 to 6 m and its length reached 8 km [41]. Diolkos was constructed in the 6th century B.C. in consideration of the need for the prompt crossing of the ships from the Saronic to the Corinth Gulf and is associated with Periander (625–585 B.C.), tyrant of Corinth. However, according to Koutsouba and Nakas [41], the frequent usage of Diolkos had already desisted after the complete destruction of Corinth (146 B.C.).

According to Morhange et al. [42], during 340 B.C., a co-seismic event provoked an uplift of Lechaion harbor by 1.2 m (6.6 km west of Diolkos) and also uplifted the entrance to Diolkos, as shown from the uplifted beachrocks that are formed on the ancient ship slipway. Below Diolkos ancient ship slipway, an older beachrock is present [43].

3. Materials and Methods

3.1. Fieldwork and Laboratory Analysis

For this work, detailed spatial mapping of Diolkos beachrock outcrops was accomplished. A differential global position system (DGPS) with global navigation satellite system (GNSS) system receiver (Spectra SP60) was used for the detailed recording of beachrock elevation/depth (with respect to the mean sea-level), length, and width of the seaward and landward parts with an accuracy of 3 cm. In total, 3 transects (AA′, BB′ and CC′) were accomplished, which also included sampling the front (seaward) and the end (landward) of each beachrock slab [12,29,44] (Figure 2).

Beachrock samples were collected from the top bed of beachrock outcrops, from the front and end slabs. Overall, 4 thin sections were prepared for petrographic and microstratigraphic analyses using a Leica DMLP (Leica Microsystems GmbH, Wetzlar, Germany) petrographic microscope with a digital camera and the corresponding image treatment software. These observations allowed characterizing the constituents, the presence/contribution of bioclasts, as well as the type of the cements and their micro-morphological features.

Figure 2. The study area of Diolkos, western part of Corinth canal. In this figure, three cross sections (AA′, BB′, CC′) are illustrated together with the location of OSL samples (DiN1, DiS1). The ancient ship trackway or slipway can be found with the dashed grey/black line.

3.2. Luminescence Dating

The beachrocks were dated by using optically stimulated luminescence (OSL) dating of quartz. Two samples were selected for dating and were processed at the Luminescence Dating Laboratory of the Institute of Physics, Silesian University of Technology, Poland. Quartz grains of 125–200 μm size were selected for use. A germanium spectrometer was used to determine the radioactivity dose rate. The determination of the equivalent dose was measured with the single aliquot regeneration protocol (OSL-SAR).

3.3. Relative Sea Level Reconstruction

For the reconstruction of the relative sea level and the production of relative sea level index points (SLIPs), we used the methodology proposed by Vacchi et al. [45], which has also been used for Mediterranean beachrocks [12,29,46]. SLIPs were produced only for those samples having intertidal formation in terms of cement typology, following the protocol proposed by Mauz et al. [10]. Cement with needles or isopachous fibers of aragonitic cement or isopachous rims and micritic high-magnesium calcite (HMC) cement or HMC cement in stalactitic position and meniscus between grains indicates that the beachrock samples have been formed in the intertidal zone [10].

The altitude of the former sea-level was estimated using the equation of Shennan & Horton [47] for each dated SLIP point. The total vertical error was obtained by adding in quadratic individual errors according to the equation:

$$e_i = (e^2{}_1 + e^2{}_2)^{1/2} \quad (1)$$

where e_1 and e_2 represent the index point error sources while taking into account both indicative range and the additional computational errors associated with the sample altitude [45].

4. Results

4.1. Beachrock Distribution

The detailed spatial mapping of the exposed beachrock of the Diolkos area was performed during summer 2020. The analysis includes the northern and southern parts of the beachrock, which is interrupted by the canal of the Corinth isthmus (Figure 3). The beachrock is composed of pile layers of sediments with plane-parallel seaward bedding. On both sides, the beachrock is highly intervened by human activity (i.e., jetties, Diolkos administration building, submerging road bridge, military installations).

Figure 3. Diolkos area beachrock outcrops. The N corresponds to the northern part and S to the southern part. The Corinth isthmus (canal) can be seen in the middle. The white dashed lines indicate the exposed Diolkos ship slipway. The areas covered by white dotted lines indicate the studied beachrock.

The beachrock, on both sides, has at least 75 cm thickness from its deepest part up to its corresponding exposed outcrop. The largest beachrock width is 105 m on the northern side. The beachrock extends to −75 cm depth and has a maximum elevation of 80 cm ± 5 cm. Due to the complexity, extensive width, and the beachrock distribution, three cross sections were carried out for better data interpretation (Figures 2 and 4).

In more detail, at the northern part, the beachrock lies at a maximum elevation of 68 ± 2 cm (Figure 4a) and maximum depth of −80 ± 2 cm (Figure 4b). In the northern part, a man-made wall structure was present almost at 23 m from the coastline. In Figure 4, the multi-banding morphology of the beachrock is evident. As is evident in Figure 4b, samples CoDi1 and CoDi2 were retrieved for microscopic analysis, as well as the sample

DiN1 for OSL dating. The northern beachrock shows a mean seaward dip of 8° from width 25–95 m, while, from 0–25 m, the mean dip is 12.5°.

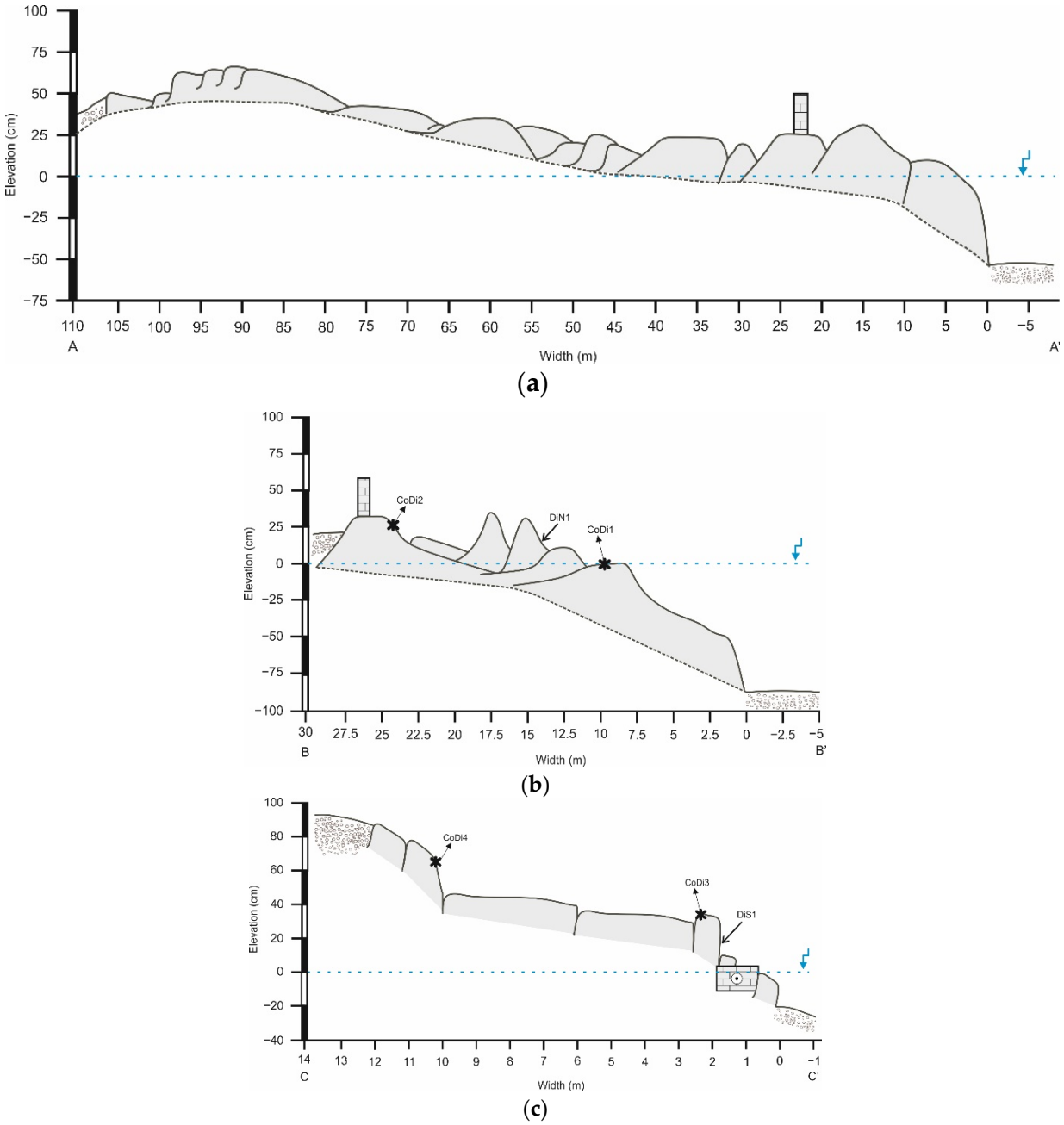

Figure 4. Schematic representation of Diolkos beachrock cross sections and sample points. The blue line represents the m.s.l. (**a**) A cross section of the northern beachrock part. At 22 m width, a wall construction is present. (**b**) A cross section of the northern beachrock part. At 26 m width, a wall construction is present. The star shaped points indicate the samples for microscopic analysis, and the arrow point at the cross section indicates the OSL dating sample. (**c**) A cross section of the southern beachrock part. At 1 m width, a Diolkos remnant is fused with the beachrock. The star shaped points indicate the samples for microscopic analysis, and the arrow point at the cross section indicates the OSL dating sample.

The southern beachrock has a maximum elevation of 83 ± 2 cm and a maximum depth of −20 ± 2 cm. The south–north cross section (Figure 4c) indicates the relationship of the beachrock and the Diolkos remnants, which are located at sea level. Another part of beachrock is submerged and below the Diolkos remnants. At this cross section, samples

CoDi3 and CoDi4 were retrieved for microscopic analysis, as well as sample DiS1 for OSL dating.

4.2. Cement Morphology and Mineralogy

All the observed Diolkos samples show a coherent pattern with sub-rounded and well to medium sorted grains with a general absence of bioclasts (<3%). The lithoclasts mainly consist of quartz, calcite, dolomite, plagioclase, and feldspar (Table 1). The examination of the beachrock cements from Diolkos showed that the micritic high magnesium calcite (HMC) [$(Ca,Mg)CO_3$] cement was the most dominant in all samples (Figure 5). In samples CoDi1 and CoDi2, the cement forms a thin isopachous coating around the sediment grains (Figure 5a,b). In samples CoDi3 and CoDi4, the cement forms a more coherent isopachous coating as well as pellet forms (Figure 5c,d). Furthermore, the CoDi4 sample has brown micritic cement, forming an outer film. A pore filling matrix cement was observed and consisted of very fine sedimentary particles (5–20 μm). Additionally, in sample CoDi4, a meniscus cement formation was noted (Figure 5).

Table 1. Mineral content and textural characteristics of beachrocks derived from the microscopical analysis and association with SLIP and indicative meaning.

Sample	Cement Type	Cement Thickness	Mineral Composition	SLIP	Indicative Meaning
CoDi1	Thin isopachous micritic HMC. No matrix and no bioclasts	<10 μm	Quartz, Mg-Calcite, Dolomite, Plagioclase, clay minerals	Intertidal, undifferentiated	MHW to MLW
CoDi2	Thin isopachous micritic HMC. No matrix and no bioclasts	<10 μm	Quartz, Mg-Calcite, Dolomite, Plagioclase, clay minerals	intertidal, undifferentiated	MHW to MLW
CoDi3	Isopachous micritic HMC and. Matrix infilling and Pellet concentrations.	10–20 μm	Quartz, Mg-Calcite, Dolomite, Plagioclase, clay minerals	Intertidal, undifferentiated	MHW to MLW
CoDi4	Isopachous micritic HMc. brown bio-micritic cement. Pellet concentrations.	10–20 μm	Quartz, Mg-Calcite, Dolomite, Plagioclase, clay minerals	Intertidal, undifferentiated	MHW to MLW

The observed binding material between the grains is mostly upper intertidal cement in samples CoDi1, CoDi2, CoDi3, and CoDi4, while the CoDi4 sample has evident forms and characteristics of freshwater influence. Cements of the upper intertidal zone are <100 μm and they are associated with detrital constituents (rock and shell fragments), which are all present in all the samples. Furthermore, the cement crystals that are forming an isopachous micritic coating serve as another indicator of intertidal zone beachrock formation. In the above samples, there was an absence of meteoric cement.

Combining the microscopic analysis and the detailed field survey, we confirmed that all the samples were beachrock samples with intertidal cement. Thus, the formation zone of the retrieved samples for OSL dating was the intertidal zone.

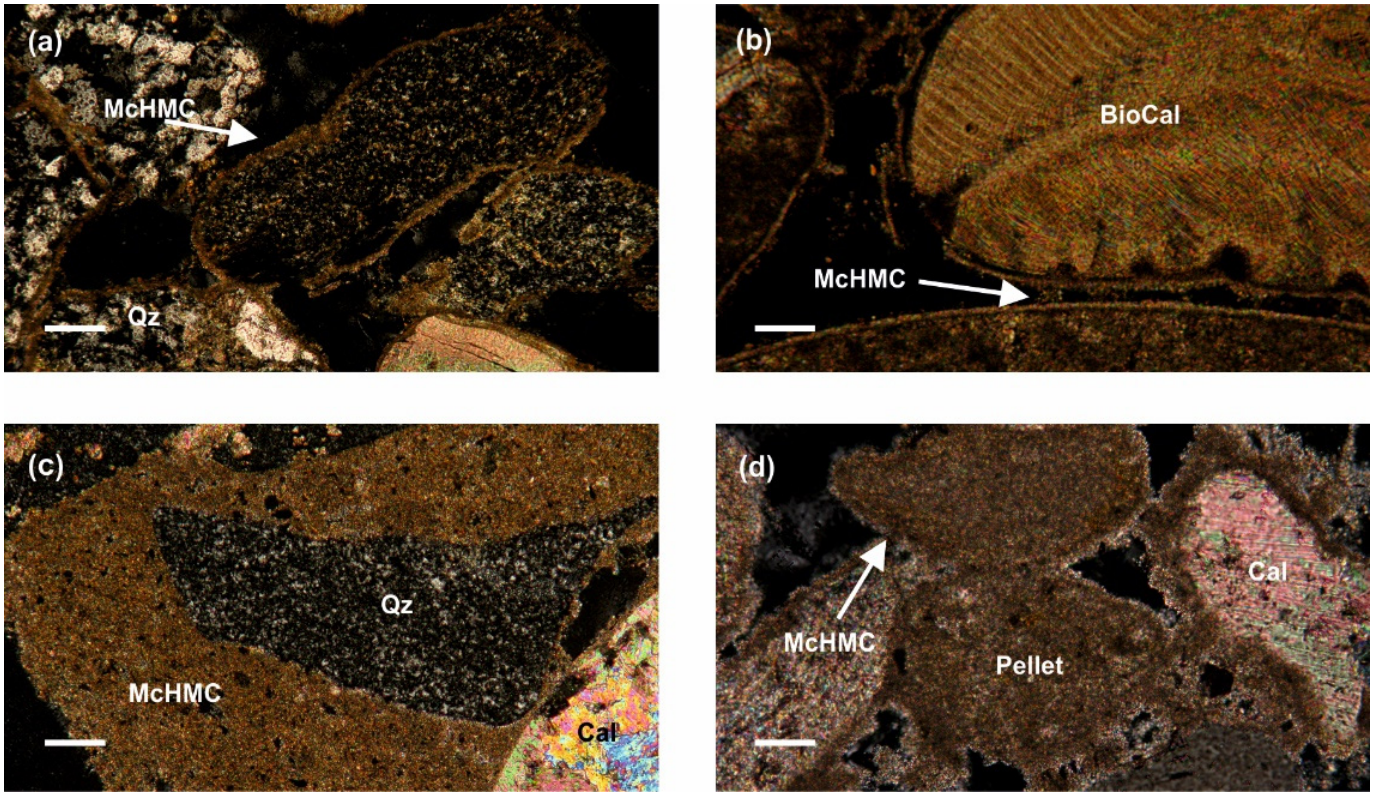

Figure 5. Polarized microscopy image in McHMC: micritic high magnesium calcite, BioCal: biogenic calcite, Cal: calcite, Qz: quartz. (**a**) Sample CoDi1, 10× magnification, scale 20 μm. Micritic HMC cement is coating mineral and lithoclast grains. (**b**) Sample CoDi2, 20× magnification, scale 10 μm. Thin micritic HMC cement is coating calcite grains. (**c**) Sample CoDi3, 20× magnification, scale 10 μm. The micritic HMC cement is fully covering the grains as a pore filling. (**d**) Sample CoDi4, 20× magnification, scale 10 μm. Micritic HMC cement is covering the sediment grains. A pellet concentration is present as a pore filling.

4.3. Sea Level Past Positions

The two samples from the northern and southern part of the beachrock were used as SLIPs. A vertical uncertainty was calculated for each index point derived from the accuracy of height measure and every possible factor associated with sampling and the later analytical processes (i.e., waves that temporally increase the water level) [29,48]. In Table 2, the OSL results of the two samples are provided. The sample DiN1 was collected from 0.17 m and the DiS1 from 0.20 m. Using the OSL dating method, we acquired the ages of 0.381 ka ± 58 years and 1.83 ka ± 14 years, respectively. Both samples were converted into SLIPs (Table 3), showing a sea level at approximately 4 cm and 8 cm, respectively. Table 3 presents all the details of converting the beachrock samples to SLIPs. Both SLIPs were acceptable as OSL dating, and the field measurements did not present methodological or any executive issues.

Table 2. Age determination results of the selected Diolkos samples.

Site	Sample Number	Elevation (m)	Method	No of Aliquots	Equivalent Dose (Gy)	Age BP (ka)
CoDiN	DiN1	0.17	Quartz	12	0.230	0.381
CoDiS	DiS1	0.20	Quartz	15	1190	1.83

Table 3. Past relative sea level calculations.

Beachrock ID	Sample No	Height (m)	Age (ka)	Tidal Range (m)	Measurement Error (m)	Indicative Meaning (m)	RWL (m)	RSL (m)	Error (cm)	Notes
CoDiN	DiN1	0.17	0.381	0.26	0.02	0.26	0.13	0.04	13	Accepted
CoDiS	DiS1	0.20	1.83	0.26	0.02	0.26	0.13	0.08	13	Accepted

5. Discussion

Coastal paleogeographic reconstructions that study sea level fluctuations during the middle–late Holocene in the Mediterranean take advantage of a variety of proxies, which include geomorphological evidence, such as tidal notches [49–52] and beachrocks [12,21,29,31,53], fixed biological indicators [54], and archaeological indicators [49,54–57]. In many studies, different proxies have been used for coastal palaeogeographical reconstructions [12,42,48].

Today, the beachrock of Diolkos is separated at its northern and southern part from the isthmus of Corinth (artificial canal), and it is uplifted. The microscopic examination of the beachrock samples revealed that their formation environment was in the upper intertidal zone [10,12,29,44,58]. The micritic HMC cement with pellet microformations, the high tendency to fill all the beachrock porosity, and the occasional brown color cement are good indicators for using a beachrock as a SLIP [9,10]. The beachrock distribution was quite complex as it had a notable width (105 m maximum), and the human interventions did not facilitate field examination.

The OSL dating was conducted on samples from the most characteristic places. It should be noted that the northern sample (DiN1) derived from the beachrock seaward face and the southern sample (DiS1) derived from the beachrock slab, exactly above the remnants of Diolkos slipway. The northern sample age was estimated at 0.381 ka $\pm$ 57 years (1569 $\pm$ 57 A.D.) and the southern sample at 1.83 ka $\pm$ 14 years (120 $\pm$ 14 A.D). These samples derived from almost the same height. However, their distances from the present-day shoreline are approximately 6 m and 60 m, respectively. Additionally, their conversion to SLIPs showed that the beachrock parts had the same relative water level during the time they were formed. Based on the aforementioned, it seems that the relative sea level did not change between 120 A.D. and 1569 A.D.

Considering the results from the beachrock mineralogical analysis, the sea level reconstruction, and the morphological analysis, it is clear that the two parts of Diolkos beachrock were once a continuous slab.

The area of Corinth isthmus has been uplifting by approximately 0.3 mm/year for the last 200 ka [59–62]. During 1981, an earthquake sequence took place at the area of Loutraki as a result of the fault system of south Alkyonides. That earthquake uplifted Corinth isthmus by 2 cm [63]. The area of Corinth isthmus is a tectonically active area given that, in the last 150 years, two strong seismic events have been described in historical records. In 1858, an earthquake of M = 6.5 destroyed Corinth, and, in 1928, an earthquake M = 6.3 inflicted extensive damage in Corinth and Loutraki [64]. The area is surrounded by a secondary faulting system that is occasionally active. At a distance of 7 km west of Diolkos, the ancient Lechaion port resides. Studies have revealed that local tectonics were responsible for producing tsunamigenic events that affected the ancient port [65,66]. Furthermore, it was noted that repeated phases of uplift and subsidence affected the area of Lechaion even if this situation is in contrast with the general geomorphological and tectonically uplifting regime of the area [66]. According to Morhange et al. [42], a tectonic uplift of 1.2 m was the main reason for the silting of the ancient port of Lechaion. It is clear that the area of Corinth is very tectonically active and the local faulting systems play an important role for the coastal geomorphological changes that affect manmade structures (e.g., ports, slipways, etc.).

Diolkos was an ancient slipway, enabling ships to cross from the Corinthian Gulf to the Saronic sea. Diolkos was constructed during the time of Periander (625–585 B.C.), tyrant of

Corinth [67]. The slipway was functional from at least the 5th to the 1st century B.C. [67]. After 67 A.D., there is no evidence of using Diolkos. At that time, Nero started the first plan to open a canal; however, his efforts failed, and the canal works were abandoned [67]. In Nero's effort to open the canal, Diolkos slipway was partly destroyed. According to Koutsouba and Nakas [41], the frequent usage of Diolkos was already in disuse after the complete destruction of Corinth (146 B.C.). Finally, the canal opening project started in 1882 and was brought to completion in 1893.

Nowadays, a submerged beachrock (hereinafter beachrock A) resides below te Diolkos remnants, which might have been used as a structural background for Diolkos construction [42]. On top of the slipway, a second beachrock exists, uplifted (hereinafter beachrock B). The beachrock A shows similar characteristics and texture with the uplifted one (Figure 6). We can assume that beachrock A had formed within the intertidal zone, similar to beachrock B.

(**a**) (**b**)

Figure 6. Southern Diolkos part. (**a**) Inland view. The dashed white line separates the beachrock B from Diolkos remnants. The erosion of Diolkos coastal zone can be observed. (**b**) Contact point of beachrock B with Diolkos remnants. From this site, the sample DiS1 was retrieved.

Our multiproxy analysis, combining historical, archaeological, geomorphological, and mineralogical data along with geochronology, allowed to reconstruct the paleogeographic evolution of Diolkos area. Before Diolkos construction (6th century B.C.), beachrock A was located in the intertidal zone. Assuming that the mean tidal range was almost the same as now, the intertidal zone was ranging between +13 cm to −13 cm. At that time, the Corinthians started constructing Diolkos on top of beachrock A, taking advantage of its slippery surface for pulling the ships. Consequently, the Diolkos slipway was located on the coastline. Beachrock A stopped its development due to the anthropogenic intervention. After the destruction of Corinth during 146 B.C., a co-seismic event must have taken place that submerged beachrock A and part of Diolkos. At that time, human intervention was limited and Diolkos ceased to be used until Nero's canal project in 64 A.D. Considering that the formation of beachrocks requires a calm coastal environment so that sand can accumulate and consequently consolidate, a new beachrock started forming after the abandonment of Nero's canal project. Morhange et al. [42] refer to a co-seismic event around 340 B.C. that might have caused an uplift in the western part of Diolkos. However, this might not be possible as, during that time, Diolkos was functional and beachrock A was still submerged.

Consequently, the first layer of beachrock B, covering the Diolkos remnants, had developed or was developing during the period of 120 ± 14 A.D. The coastal zone had found again its natural equilibrium as the longshore drift currents from Loutraki and Corinth supplied Diolkos with fresh sediment.

Beachrock B started developing and increasing its width and thickness at least up until 1569 ± 57 A.D. After that time, at least one co-seismic event may have occurred, which uplifted the area by ~12 cm. Between 1569 and the Corinth canal opening in 1882,

the beachrock may have been still developing (Figure 7). Taking into account the seismic events of 1858 and 1928, we may assume that these events may have uplifted the Diolkos area.

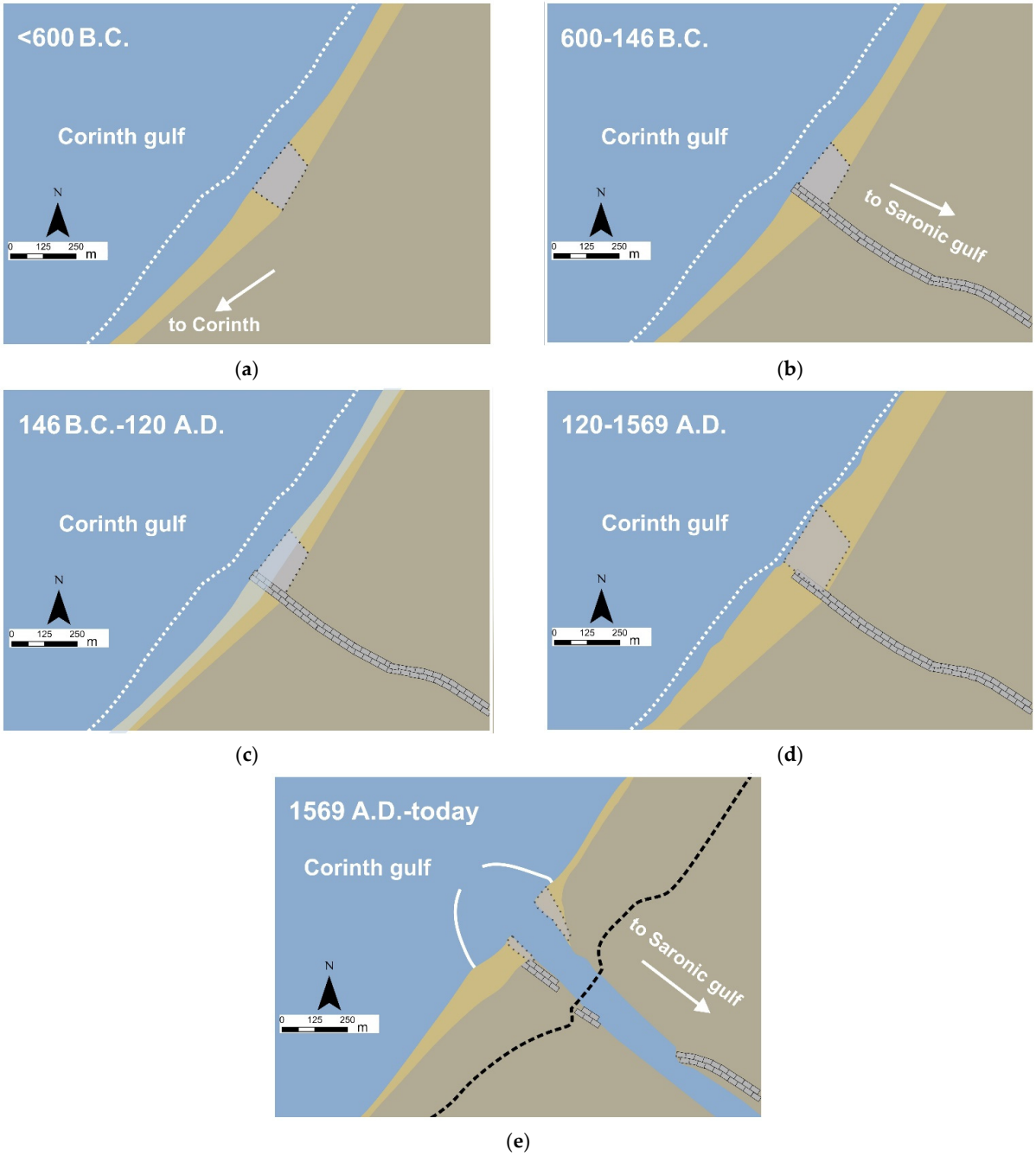

Figure 7. An illustration of the paleogeographic evolution of Diolkos area before the slipway construction until today. The white dashed line indicates the modern coast, the grey rectangle indicates the formed beachrocks, the grey blocks indicate Diolkos slipway, the black dashed line indicates the modern road of Posidonia, and the white lines indicate jetties. (**a**) The coastal zone of Diolkos area before the construction of the slipway (<600 B.C.), indicating the beachrock A. (**b**) Construction of Diolkos slipway on the beachrock A. (**c**) Subsidence of beachrock A and Diolkos slipway. (**d**) The new sediments overlay Diolkos slipway and form the beachrock B. The coast has advanced towards se€. (**e**) The coast reached today's position as the Corinth canal has been opened, and the majority of the beachrock is destroyed.

The functional height of an archaeological remain corresponds to the position (height) of specific architectural parts in relation to the mean sea level at the time of construction. Functional heights set the minimum construction height above the highest local tide [49,68]. There are few studies that refer to the functional height of ancient slipways. In Morhange and Marriner [69], several archaeological sea level indicators were studied along with slipways, which were categorized as meso-tidal functional constructions. Anzidei et al. [70] mentioned that the slipway of Carthage, Tunisia is less constrained as a sea level marker with a functional height of 0.24 ± 0.5 m. Baika [71] investigated a submerged slipway from Kea island, Cyclades, Greece of the Classical/Hellenistic era and identified the relevant RSL of the construction, around −2 to 2.5 ± 0.3 m. Diolkos was constructed by limestone blocks of 35 cm thickness. Taking into account the available literature and the possible Diolkos building material, we can assume that the subsidence of the beachrock A and Diolkos remnants was of the order of ~35 ± 16 cm.

6. Conclusions

In this study, we investigated the evolution of the Diolkos, Corinth, Greece beachrock. Combining data from the geomorphological field study, mineralogical and microscopic analysis, OSL dating, and historical and archaeological records, the paleogeography of the Diolkos area was possible.

- Before the 6th century B.C., a beachrock was lying on the intertidal zone covering the area and reaching at least 65 m from today's coastline.
- Diolkos construction occurred and the beachrock stopped its development until the destruction of Corinth in 146 B.C.
- A subsidence occurred totaling 35 ± 16 cm, and Diolkos along with beachrock A were submerged.
- Sediment accumulation occurred after Nero's intervention at 67 A.D., forming a new beachrock in the intertidal zone in 120 ± 14 A.D.
- After 120 ± 14 A.D., the beachrock continued its development up until 1569 ± 57 A.D.
- After 1569 ± 57 A.D., the beachrock developed another 5 m width until the present-day coastline. The area uplifted by 12 cm owing to one or more co-seismic events.
- The beachrock development stopped when the Corinth canal construction started in 1882.

Author Contributions: Conceptualization, G.S. and N.E.; methodology, G.S., A.K. and N.E.; investigation, G.S.; writing—original draft preparation, G.S. and A.K.; writing—review and editing, G.S., A.K., N.E. and H.M.; visualization, G.S.; supervision, N.E. All authors have read and agreed to the published version of the manuscript.

Funding: This research received no external funding.

Institutional Review Board Statement: Not applicable.

Informed Consent Statement: Not applicable.

Conflicts of Interest: The authors declare no conflict of interest.

References

1. Khan, N.S.; Ashe, E.; Shaw, T.A.; Vacchi, M.; Walker, J.; Peltier, W.R.; Kopp, R.E.; Horton, B.P. Holocene Relative Sea-Level Changes from Near-, Intermediate-, and Far-Field Locations. *Curr. Clim. Chang. Rep.* **2015**, *1*, 247–262. [CrossRef]
2. Rovere, A.; Raymo, M.E.; Vacchi, M.; Lorscheid, T.; Stocchi, P.; Gómez-Pujol, L.; Harris, D.L.; Casella, E.; O'Leary, M.J.; Hearty, P.J. The analysis of Last Interglacial (MIS 5e) relative sea-level indicators: Reconstructing sea-level in a warmer world. *Earth-Sci. Rev.* **2016**, *159*, 404–427. [CrossRef]
3. Engelhart, S.E.; Horton, B.P.; Douglas, B.C.; Peltier, W.R.; Törnqvist, T.E. Spatial variability of late Holocene and 20th century sea-level rise along the Atlantic coast of the United States. *Geology* **2009**, *37*, 1115–1118. [CrossRef]
4. Stattegger, K.; Tjallingii, R.; Saito, Y.; Michelli, M.; Trung Thanh, N.; Wetzel, A. Mid to late Holocene sea-level reconstruction of Southeast Vietnam using beachrock and beach-ridge deposits. *Glob. Planet. Change* **2013**, *110*, 214–222. [CrossRef]

5. Tsanakas, K.; Karymbalis, E.; Cundy, A.; Gaki-Papanastassiou, K.; Papanastasiou, D.; Drinia, H.; Koskeridou, E.; Maroukian, H. Late Holocene geomorphic evolution of the Livadi coastal plain, Gulf of Argostoli, Cephalonia Island, Western Greece. *Geogr. Fis. Din. Quat.* **2019**, *42*, 43–60. [CrossRef]
6. Melis, R.T.; Di Rita, F.; French, C.; Marriner, N.; Montis, F.; Serreli, G.; Sulas, F.; Vacchi, M. 8000 years of coastal changes on a western Mediterranean island: A multiproxy approach from the Posada plain of Sardinia. *Mar. Geol.* **2018**, *403*, 93–108. [CrossRef]
7. Caporizzo, C.; Gracia, F.J.; Aucelli, P.P.C.; Barbero, L.; Martín-Puertas, C.; Lagóstena, L.; Ruiz, J.A.; Alonso, C.; Mattei, G.; Galán-Ruffoni, I.; et al. Late-Holocene evolution of the Northern Bay of Cádiz from geomorphological, stratigraphic and archaeological data. *Quat. Int.* **2021**, *602*, 92–109. [CrossRef]
8. Seeliger, M.; Pint, A.; Frenzel, P.; Marriner, N.; Spada, G.; Vacchi, M.; Başaran, S.; Dan, A.; Seeger, F.; Seeger, K.; et al. Mid- to late-Holocene sea-level evolution of the northeastern Aegean sea. *Holocene* **2021**, *31*, 1621–1634. [CrossRef]
9. Vousdoukas, M.I.; Velegrakis, A.F.; Plomaritis, T.A. Beachrock occurrence, characteristics, formation mechanisms and impacts. *Earth-Sci. Rev.* **2007**, *85*, 23–46. [CrossRef]
10. Mauz, B.; Vacchi, M.; Green, A.; Hoffmann, G.; Cooper, A. Beachrock: A tool for reconstructing relative sea level in the far-field. *Mar. Geol.* **2015**, *362*, 1–16. [CrossRef]
11. Danjo, T.; Kawasaki, S. Characteristics of Beachrocks: A Review. *Geotech. Geol. Eng.* **2014**, *32*, 215–246. [CrossRef]
12. Karkani, A.; Evelpidou, N.; Vacchi, M.; Morhange, C.; Tsukamoto, S.; Frechen, M.; Maroukian, H. Tracking shoreline evolution in central Cyclades (Greece) using beachrocks. *Mar. Geol.* **2017**, *388*, 25–37. [CrossRef]
13. Tucker, M.E.; Bathurst, R.G.C. *Carbonate Diagenesis*; Blackwell Publishing Ltd.: Oxford, UK, 1990.
14. Gischler, E. Beachrock and Intertidal Precipitates. In *Geochemical Sediments and Landscapes*; Blackwell Publishing Ltd.: Hoboken, NJ, USA, 2008; pp. 365–390. ISBN 9781405125192.
15. Alexandersson, T. Intragranular Growth of Marine Aragonite and Mg-Calcite: Evidence of Precipitation from Supersaturated Seawater. *J. Sediment. Res.* **1972**, *42*, 441–460. [CrossRef]
16. Scholle, P.A.; Bebout, D.G.; Moore, C.H. *Carbonate Depositional Environments*; Scholle, P.A., Bebout, D.G., Moore, C.H., Eds.; The American Association of Petroleum Geologists: Tulsa, Oklahoma, 1983; ISBN 0891813101.
17. Kelletat, D. Beachrock as Sea-Level Indicator? Remarks from a Geomorphological Point of View. *J. Coast. Res.* **2006**, *226*, 1558–1564. [CrossRef]
18. Desruelles, S.; Fouache, É.; Ciner, A.; Dalongeville, R.; Pavlopoulos, K.; Kosun, E.; Coquinot, Y.; Potdevin, J.-L. Beachrocks and sea level changes since Middle Holocene: Comparison between the insular group of Mykonos–Delos–Rhenia (Cyclades, Greece) and the southern coast of Turkey. *Glob. Planet. Change* **2009**, *66*, 19–33. [CrossRef]
19. Evelpidou, N.; Kampolis, I.; Pirazzoli, P.A.; Vassilopoulos, A. Global sea-level rise and the disappearance of tidal notches. *Glob. Planet. Change* **2012**, *92–93*, 248–256. [CrossRef]
20. Vacchi, M.; Rovere, A.; Zouros, N.; Desruelles, S.; Caron, V.; Firpo, M. Spatial distribution of sea-level markers on Lesvos Island (NE Aegean Sea): Evidence of differential relative sea-level changes and the neotectonic implications. *Geomorphology* **2012**, *159–160*, 50–62. [CrossRef]
21. Falkenroth, M.; Schneider, B.; Hoffmann, G. Beachrock as sea-level indicator—A case study at the coastline of Oman (Indian Ocean). *Quat. Sci. Rev.* **2019**, *206*, 81–98. [CrossRef]
22. Alexandrakis, G.; Petrakis, S.; Kampanis, N.A. Integrating geomorphological data, geochronology and archaeological evidence for coastal landscape reconstruction, the case of Ammoudara Beach, Crete. *Water* **2021**, *13*, 1269. [CrossRef]
23. Alexandersson, T. Recent littoral and sublittoral high-mg calcite lithification in the mediterranean. *Sedimentology* **1969**, *12*, 47–61. [CrossRef]
24. Neumeier, U. Experimental modelling of beachrock cementation under microbial influence. *Sediment. Geol.* **1999**, *126*, 35–46. [CrossRef]
25. Psomiadis, D.; Tsourlos, P.; Albanakis, K. Electrical resistivity tomography mapping of beachrocks: Application to the island of Thassos (N. Greece). *Environ. Earth Sci.* **2009**, *59*, 233–240. [CrossRef]
26. Nikolakopoulos, K.; Lampropoulou, P.; Fakiris, E.; Sardelianos, D.; Papatheodorou, G. Synergistic Use of UAV and USV Data and Petrographic Analyses for the Investigation of Beachrock Formations: A Case Study from Syros Island, Aegean Sea, Greece. *Minerals* **2018**, *8*, 534. [CrossRef]
27. Hopley, D. Beachrock as a sea-level indicator. In *Sea-Level Research*; van der Plassche, O., Ed.; Springer: Dordrecht, The Netherlands, 1986; pp. 157–173.
28. Evelpidou, N. Geomorphology and Sea Level. In *Encyclopedia of Coastal Science*; Finkl, C., Makowski, C., Eds.; Springer: Cham, Switzerland, 2019; pp. 885–894. ISBN 9783319486574.
29. Polidorou, M.; Saitis, G.; Evelpidou, N. Beachrock development as an indicator of paleogeographic evolution, the case of Akrotiri Peninsula, Cyprus. *Z. Geomorphol.* **2021**, *63*, 3–17. [CrossRef]
30. Erginal, A.E.; Kıyak, N.G.; Öztürk, B. Investigation of Beachrock Using Microanalyses and OSL Dating: A Case Study from Bozcaada Island, Turkey. *J. Coast. Res.* **2010**, *262*, 350–358. [CrossRef]
31. Ozturk, M.Z.; Erginal, A.E.; Kiyak, N.G.; Ozturk, T. Cement fabrics and optical luminescence ages of beachrock, North Cyprus: Implications for Holocene sea-level changes. *Quat. Int.* **2016**, *401*, 132–140. [CrossRef]
32. Tatumi, S.H.; Kowate, E.A.; Gozzi, G.; Kassab, L.R.P.; Suguio, K.; Barreto, A.M.F.; Bezerra, F. Optical dating results of beachrock, eolic dunes and sediments applied to sea-level changes study. *J. Lumin.* **2003**, *102–103*, 562–565. [CrossRef]

33. Barreto, A.M.F.; Bezerra, F.H.R.; Suguio, K.; Tatumi, S.H.; Yee, M.; Paiva, R.P.; Munita, C.S. Late Pleistocene marine terrace deposits in northeastern Brazil: Sea-level change and tectonic implications. *Palaeogeogr. Palaeoclimatol. Palaeoecol.* **2002**, *179*, 57–69. [CrossRef]
34. Thomas, P.J. Luminescence Dating of Beachrock in the Southeast Coast of India—Potential for Holocene Shoreline Reconstruction. *J. Coast. Res.* **2009**, *251*, 1–7. [CrossRef]
35. Papanikolaou, D. Tectonostratigraphic models of the Alpine terranes and subduction history of the Hellenides. *Tectonophysics* **2013**, *595–596*, 1–24. [CrossRef]
36. Higgins, M.D.; Higgins, R.A. A geological companion to Greece and the Aegean. *Choice Rev.* **1993**, 34–3874. [CrossRef]
37. Papanikolaou, D.J.; Royden, L.H. Disruption of the Hellenic arc: Late Miocene extensional detachment faults and steep Pliocene-Quaternary normal faults—Or what happened at Corinth? *Tectonics* **2007**, *26*, TC5003. [CrossRef]
38. Hellenic Navy Hydrographic Service. *Hellenic Navy Hydrographic Service*; Hellenic Navy Hydrographic Service: Athens, Greece, 2015.
39. Verdelis, N. Continuation of Diolkos excavation. *Archaeol. Newsp.* **1956**, *95*, 1–3.
40. Verdelis, N. Diolkos excavation. In *Practicals of the Archaeological Society of Athens*; Archaeological Society at Athens 1960; Archaeological Society of Athens: Athens, Greece, 1960; Volume 160, pp. 136–143.
41. Koutsouba, D.; Nakas, G. Diolkos: A significant engineering structure of Antiquity. In Proceedings of the Corinthia and the Northeast Peloponnesus, Loutraki, Greece, 26–29 March 2009.
42. Morhange, C.; Pirazzoli, P.A.; Evelpidou, N.; Marriner, N. Late Holocene Tectonic Uplift and the Silting Up of Lechaion, the Western Harbor of Ancient Corinth, Greece. *Geoarchaeology* **2012**, *27*, 278–283. [CrossRef]
43. Maroukian, H.; Gaki-Papanastassiou, K.; Papanastassiou, D. Coastal changes in Corinthia, Greece. In *RES MARITIMAE: Cyprus and the Eastern Mediterranean from Prehistory to Late Antiquity*; Swiny, S., Hohlfelder, R.L., WyldeSwiny, H., Eds.; Scholars Press: Atlanta, GA, USA, 1994; pp. 217–226.
44. Saitis, G.; Koutsopoulou, E.; Karkani, A.; Anastasatou, M.; Stamatakis, M.; Gatou, M.-A.; Evelpidou, N. A multi-analytical study of beachrock formation in Naxos and Paros Islands, Aegean Sea, Greece and their palaeoenvironmental significance. *Z. Geomorphol.* **2021**, *63*, 19–32. [CrossRef]
45. Vacchi, M.; Marriner, N.; Morhange, C.; Spada, G.; Fontana, A.; Rovere, A. Multiproxy assessment of Holocene relative sea-level changes in the western Mediterranean: Sea-level variability and improvements in the definition of the isostatic signal. *Earth-Sci. Rev.* **2016**, *155*, 172–197. [CrossRef]
46. Vacchi, M.; Ghilardi, M.; Spada, G.; Currás, A.; Robresco, S. New insights into the sea-level evolution in Corsica (NW Mediterranean) since the late Neolithic. *J. Archaeol. Sci. Rep.* **2017**, *12*, 782–793. [CrossRef]
47. Shennan, I.; Horton, B. Holocene land- and sea-level changes in Great Britain. *J. Quat. Sci.* **2002**, *17*, 511–526. [CrossRef]
48. Dean, S.; Horton, B.P.; Evelpidou, N.; Cahill, N.; Spada, G.; Sivan, D. Can we detect centennial sea-level variations over the last three thousand years in Israeli archaeological records? *Quat. Sci. Rev.* **2019**, *210*, 125–135. [CrossRef]
49. Evelpidou, N.; Pirazzoli, P.; Vassilopoulos, A.; Spada, G.; Ruggieri, G.; Tomasin, A. Late Holocene Sea Level Reconstructions Based on Observations of Roman Fish Tanks, Tyrrhenian Coast of Italy. *Geoarchaeology* **2012**, *27*, 259–277. [CrossRef]
50. Evelpidou, N.; Melini, D.; Pirazzoli, P.A.; Vassilopoulos, A. Evidence of repeated late Holocene rapid subsidence in the SE Cyclades (Greece) deduced from submerged notches. *Int. J. Earth Sci.* **2014**, *103*, 381–395. [CrossRef]
51. Boulton, S.J.; Stewart, I.S. Holocene coastal notches in the Mediterranean region: Indicators of palaeoseismic clustering? *Geomorphology* **2015**, *237*, 29–37. [CrossRef]
52. Sisma-Ventura, G.; Sivan, D.; Shtienberg, G.; Bialik, O.M.; Filin, S.; Greenbaum, N. Last interglacial sea level high-stand deduced from well-preserved abrasive notches exposed on the Galilee coast of northern Israel. *Palaeogeogr. Palaeoclimatol. Palaeoecol.* **2017**, *470*, 1–10. [CrossRef]
53. Damien, A.; Kosmas, P.; Éric, F. Holocene relative sea-level variations and archeological implications, Abu Dhabi western region, United Arab Emirates. *Arab. J. Geosci.* **2020**, *13*, 1–16. [CrossRef]
54. Vacchi, M.; Russo Ermolli, E.; Morhange, C.; Ruello, M.R.; Di Donato, V.; Di Vito, M.A.; Giampaola, D.; Carsana, V.; Liuzza, V.; Cinque, A.; et al. Millennial variability of rates of sea-level rise in the ancient harbour of Naples (Italy, western Mediterranean Sea). *Quat. Res.* **2020**, *93*, 284–298. [CrossRef]
55. Sivan, D.; Widowinski, S.; Lambeck, K.; Galili, E.; Raban, A. Holocene sea-level changes along the Mediterranean coast of Israel, based on archaeological observations and numerical model. *Palaeogeogr. Palaeoclim. Palaeoecol.* **2001**, *167*, 101–117. [CrossRef]
56. Sivan, D.; Lambeck, K.; Toueg, R.; Raban, A.; Porath, Y.; Shirman, B. Ancient coastal wells of Caesarea Maritima, Israel, an indicator for relative sea level changes during the last 2000 years. *Earth Planet. Sci. Lett.* **2004**, *222*, 315–330. [CrossRef]
57. Benjamin, J.; Rovere, A.; Fontana, A.; Furlani, S.; Vacchi, M.; Inglis, R.H.; Galili, E.; Antonioli, F.; Sivan, D.; Miko, S. Late Quaternary sea-level changes and early human societies in the central and eastern Mediterranean Basin: An interdisciplinary review. *Q. Int.* **2017**, *449*, 29–57. [CrossRef]
58. Petropoulos, A.; Baziotis, I.; Anagnostou, C.; Evelpidou, N. Beachrocks cement characteristics and conditions of formation. case study platanias beach, chania, greece. *Bull. Geol. Soc. Greece* **2017**, *50*, 458. [CrossRef]
59. Collier, R.E.L.; Leeder, M.R.; Rowe, P.J.; Atkinson, T.C. Rates of tectonic uplift in the Corinth and Megara Basins, central Greece. *Tectonics* **1992**, *11*, 1159–1167. [CrossRef]

60. Dia, A.N.; Cohen, A.S.; O'Nions, R.K.; Jackson, J.A. Rates of uplift investigated through 230Th dating in the Gulf of Corinth (Greece). *Chem. Geol.* **1997**, *138*, 171–184. [CrossRef]
61. Turner, J.A.; Leeder, M.R.; Andrews, J.E.; Rowe, P.J.; van Calsteren, P.V.; Thomas, L. Testing rival tectonic uplift models for the Lechaion Gulf in the Gulf of Corinth rift. *J. Geol. Soc.* **2010**, *167*, 1237–1250. [CrossRef]
62. Papanikolaou, I.D.; Triantaphyllou, M.; Pallikarakis, A.; Migiros, G. Active faulting at the Corinth Canal based on surface observations, borehole data and paleoenvironmental interpretations. Passive rupture during the 1981 earthquake sequence? *Geomorphology* **2015**, *237*, 65–78. [CrossRef]
63. Mariolakos, I.; Stiros, S.C. Quaternary deformation of the Isthmus and Gulf of Corinthos (Greece). *Geology* **1987**, *15*, 225–228. [CrossRef]
64. Papazachos, B.P.; Papazachou, C.B. *The Earthquakes of Greece*; Ziti Publ.: Thessaloniki, Greece, 1997; p. 304.
65. Hadler, H.; Koster, B.; Mathes-schmidt, M. Lechaion, the Ancient Harbour of Corinth (Peloponnese, Greece) destroyed by tsunamigenic impact. In Proceedings of the 2nd INQUA-IGCP-567 International Workshop on Active Tectonics, Earthquake Geology, Archaeology and Engineeering, Corinth, Greece, 19–24 September 2011; p. 1755.
66. Hadler, H.; Vött, A.; Koster, B.; Mathes-Schmidt, M.; Mattern, T.; Ntageretzis, A.K.; Reicherter, K.; Willershäuser, T. Multiple late-Holocene tsunami landfall in the eastern Gulf of Corinth recorded in the palaeotsunami geo-archive at Lechaion, harbour of ancient Corinth (Peloponnese, Greece). *Z. Geomorphol. Suppl. Issues* **2013**, *57*, 139–180. [CrossRef]
67. Lewis, M.J.T. Railways in the Greek and Roman world in Early Railways. In *Early Railways. A Selection of Papers from the First International Early Railways Conference*; Guy, A., Ed.; Newcomen Society: London, UK, 2001; pp. 8–19.
68. Lambeck, K.; Anzidei, M.; Antonioli, F.; Benini, A.; Esposito, A. Sea level in Roman time in the Central Mediterranean and implications for recent change. *Earth Planet. Sci. Lett.* **2004**, *224*, 563–575. [CrossRef]
69. Morhange, C.; Marriner, N. Archeological and biological relative sea-level indicators. *Handb. Sea-Level Res.* **2015**, 146–156. [CrossRef]
70. Anzidei, M.; Antonioli, F.; Lambeck, K.; Benini, A.; Soussi, M.; Lakhdar, R. New insights on the relative sea level change during Holocene along the coasts of Tunisia and western Libya from archaeological and geomorphological markers. *Quat. Int.* **2011**, *232*, 5–12. [CrossRef]
71. Baika, K. Archaeological indicators of relative sea-level changes in the Attico-Cycladic massif: Preliminary results. *Bull. Geol. Soc. Greece* **2008**, *XLII*, 33–48.